

# Towards optimization of the Josephson diode effect

Michiyasu Mori,<sup>1,\*</sup> Wataru Koshibae,<sup>2</sup> and Sadamichi Maekawa<sup>1,2,3</sup>

<sup>1</sup>*Advanced Science Research Center, Japan Atomic Energy Agency, Tokai, Ibaraki 117-1195, Japan*

<sup>2</sup>*RIKEN Center for Emergent Matter Science (CEMS), Wako 351-0198, Japan*

<sup>3</sup>*Kavli Institute for Theoretical Sciences, University of Chinese Academy of Sciences, Beijing 100049, China*

(Dated: January 31, 2025)

We theoretically study the Josephson diode effect in the junction of singlet superconductors separated by the Rashba system in the in-plane magnetic field perpendicular to the bias current. The coupling energy of two superconductors is formulated under the bias current using a tunneling Hamiltonian with a one-dimensional model. The bias current shifts the Fermi momentum in the Rashba system due to the continuity of the electronic current. Including the shift of Fermi momentum in the coupling energy, it is found that the critical current is asymmetric with respect to the current and the magnetic field, i.e., Josephson diode effect. Depending on a distance between the superconducting electrodes  $d$ , the Josephson diode effect changes its magnitude and sign. The magnitude is inversely proportional to a band split caused by the spin-orbit interaction. Since  $d$  is experimentally controllable, the Josephson diode effect can be optimized by tuning of  $d$ . Our theory develops a new guiding principle to design the Josephson diode device.

## I. INTRODUCTION

The superconducting diode effect is a phenomenon whereby the superconducting critical current ( $I_c$ ) depends on the direction of an applied current in a magnetic field. The asymmetry of  $I_c$  has been observed in a metal-semiconductor multilayer and is associated with an asymmetric flux flow [1, 2]. The superconducting diode effect has also been reported using a high- $T_c$  cuprate/ferromagnetic manganese heterostructure for magnetic memory applications [3]. Recently, Ando et al. have reported the superconducting diode effect in the multilayer composed of three elements, i.e., Nb, Ta, and V without an inversion center [4, 5]. They have reported that their superconducting diode effect arises from the magnetochiral anisotropy effect induced by a spin-orbit interaction. This is different from the flux flow mechanism and has inspired many studies of the superconducting diode effect [6–8]. The theoretical studies propose that the superconducting diode effect is caused by the spatial variation of the superconducting order parameter, e.g., helical superconductor, due to the spin-orbit interaction [9–13].

Motivated by the superconducting diode effect, the non-reciprocity of  $I_c$  in Josephson junctions is also studied experimentally [14–19]. A typical device consists of two superconducting electrodes coupled via a two dimensional electron system with a spin-orbit interaction, i.e., Rashba system [20, 21]. The current-voltage curve of Josephson junction is measured by applying a current  $I_B$ . When the in-plane magnetic field perpendicular to  $I_B$  is simultaneously applied to the Rashba system (See Fig. 1 (a)),  $I_c$  with positive current ( $I_c^+$ ) is different from  $I_c$  with negative current ( $I_c^-$ ), i.e.,  $I_c^+ \neq I_c^-$  (See Fig. 1 (b)). The phenomenon is reversed by reversing the di-

rection of the magnetic field. We call it Josephson diode effect instead of the superconducting diode effect.

Theoretically, the Josephson junction via the Rashba system with a magnetic field was studied by Bezuglyi et al. [22], although the Josephson diode effect was not addressed. They reported  $I_c$  oscillates with the magnetic field or the distance of superconducting electrodes,  $d$ . This is the same mechanism as the superconductor/ferromagnet/superconductor (SFS) junction [23, 24], in which  $I_c$  changes its sign with  $d$  [25–34]. The negative  $I_c$  means that the current-phase relation shifted by  $\pi$ , i.e., the  $\pi$ -junction [23, 24]. It is expected to provide various applications for classical digital logic elements and flux-bias-free flux qubit [35, 36]. The distance between superconductors essentially changes the transport property of Josephson junction and opens a new pathway for the application.

The Josephson diode effect has been theoretically studied by many authors [37–53]. In those studies, the Josephson diode effect was discussed as the asymmetric current-phase relation due to the spin-orbit interaction in the presence of the Josephson coupling energy involving higher harmonics as a function of the phase. Yokoyama et al. numerically examined the asymmetric current-phase relation and reported the directional dependence of the critical current [38]. The Andreev bound state is examined to calculate the current phase relation of the junction with a transparent interface [40, 42–46]. The  $d$ -dependence of the Josephson diode effect was discussed in the references [43, 51]. However, the previous studies did not include the bias current explicitly in their formulation. The Josephson diode effect occurs as the response to the bias current. Therefore, including the bias current into the formulation is important to study the Josephson diode effect.

In this paper, we study the Josephson diode effect in the junction of two singlet superconductors separated by the Rashba system with distance  $d$ . The coupling energy of two superconductors is formulated under the

\* E-mail: mori.michiyasu@jaea.go.jp

bias current using a tunneling Hamiltonian with a one-dimensional model. The bias current is of crucial importance for the Josephson diode effect. In the Rashba system, the bias current is described by shift of the Fermi momentum due to the continuity of the electronic current. By including the bias current in the formulation, the first harmonic of the Josephson coupling reproduces the Josephson diode effect. Our analytical results suggest that the magnitude and the sign of  $I_c^+ - I_c^-$  depends on  $d$ . It will be useful to develop a new guiding principle to design the Josephson diode device.

This paper is organized as follows: Sec. II presents the model and Hamiltonian; Sec. III provides a coupling energy of the junction in the fourth order of tunneling matrix element; Sec. IV, the Josephson diode effect is examined by calculating the coupling energy with the applied current. We show the  $d$ -dependence of the Josephson diode effect. Sec. V provides a summary. The reduced Planck constant  $\hbar$  and the Boltzmann constant  $k_B$  are taken to be unity.

## II. HAMILTONIAN: LINEARIZED ONE-DIMENSIONAL MODEL

The Josephson junction separated by the Rashba system is illustrated in Fig. 1 (a). Under the in-plane magnetic field  $h_y$  perpendicular to  $I_B$ ,  $I_c$  in the positive branch  $I_c^+$  (red) is different from  $I_c$  in the negative branch  $I_c^-$  (blue) as shown in Fig. 1 (b). The difference between  $I_c^+$  and  $I_c^-$ , i.e.,  $I_c^+ - I_c^-$ , is reversed by reversing  $I_B$  or

$h_y$ . Therefore, the Josephson diode effect is characterized by  $I_c^+ - I_c^- \propto I_B \cdot h_y$  [54].  $I_c$  of Josephson junction is calculated using the Josephson coupling energy between two superconductors (SCs). The current-phase relation is also derived by taking the derivative of the coupling energy with respect to the phase difference of two SCs. In order to obtain an analytical formula of the coupling energy, we use a one-dimensional model, in which the dispersion relation of electrons is linearized around the Fermi momentum  $\pm k_F$ .

The Hamiltonian of singlet SC in left (SC<sub>L</sub>,  $\lambda = L$ ) and right (SC<sub>R</sub>,  $\lambda = R$ ) electrode is given by,

$$\begin{aligned}
H_\lambda &= \sum_{k,\sigma=\pm} \left[ v_F (k - k_F) a_{\lambda k\sigma}^\dagger a_{\lambda k\sigma} - v_F (k + k_F) b_{\lambda k\sigma}^\dagger b_{\lambda k\sigma} \right] \\
&+ \sum_{k,\sigma=\pm} \left[ v_F (k + k_F) a_{\lambda \bar{k}\sigma}^\dagger a_{\lambda \bar{k}\sigma} - v_F (k - k_F) b_{\lambda \bar{k}\sigma}^\dagger b_{\lambda \bar{k}\sigma} \right] \\
&+ \sum_{k,\sigma=\pm} \left[ \sigma \Delta \left( a_{\lambda k\sigma}^\dagger b_{\lambda \bar{k}\bar{\sigma}}^\dagger + b_{\lambda k\sigma}^\dagger a_{\lambda \bar{k}\bar{\sigma}}^\dagger \right) \right. \\
&\quad \left. - \sigma \Delta^* \left( b_{\lambda \bar{k}\bar{\sigma}} a_{\lambda k\sigma} + a_{\lambda \bar{k}\bar{\sigma}} b_{\lambda k\sigma} \right) \right], \quad (1) \\
\Delta &\equiv \mathcal{I} \langle a_{\lambda k+} b_{\lambda \bar{k}-} - a_{\lambda k-} b_{\lambda \bar{k}+} \rangle, \quad (2)
\end{aligned}$$

with momentum  $k$  ( $\bar{k} \equiv -k$ ), Fermi velocity  $v_F$ , and electrons spin  $\sigma$  ( $\bar{\sigma} \equiv -\sigma$ ). The singlet superconducting state by interaction  $\mathcal{I}$  is assumed in the both electrodes. The electron creation (annihilation) operators around  $+k_F$  and  $-k_F$  are denoted by  $a_{\lambda k\sigma}^\dagger$  and  $b_{\lambda k\sigma}^\dagger$  ( $a_{\lambda k\sigma}$  and  $b_{\lambda k\sigma}$ ), respectively.

In our theory, the Rashba system is introduced by the following one-dimensional model,

$$H_M = H_1 + H_2 + H_3 + H_4 \quad (3)$$

$$H_1 = \sum_{k,\sigma,\sigma'} a_{k\sigma}^\dagger \{ [v_F (k - k_F) - \gamma h_z \tau_{3\sigma\sigma'}] - (\alpha_R k_F - \gamma h_y) \tau_{2\sigma\sigma'} \} a_{k\sigma'} \quad (4)$$

$$H_2 = \sum_{k,\sigma,\sigma'} b_{k\sigma}^\dagger \{ [-v_F (k + k_F) - \gamma h_z \tau_{3\sigma\sigma'}] + (\alpha_R k_F + \gamma h_y) \tau_{2\sigma\sigma'} \} b_{k\sigma'} \quad (5)$$

$$H_3 = \sum_{k,\sigma,\sigma'} a_{\bar{k}\sigma}^\dagger \{ [v_F (k + k_F) + \gamma h_z \tau_{3\sigma\sigma'}] + (\alpha_R k_F - \gamma h_y) \tau_{2\sigma\sigma'} \} a_{\bar{k}\sigma'}^\dagger \quad (6)$$

$$H_4 = \sum_{k,\sigma,\sigma'} b_{\bar{k}\sigma}^\dagger \{ [-v_F (k - k_F) + \gamma h_z \tau_{3\sigma\sigma'}] - (\alpha_R k_F + \gamma h_y) \tau_{2\sigma\sigma'} \} b_{\bar{k}\sigma'}^\dagger, \quad (7)$$

with the Pauli matrix  $\tau_n$  ( $n = 1, 2, 3$ ), external magnetic field in  $y$  ( $z$ ) direction  $h_y$  ( $h_z$ ), and a Rashba parameter  $\alpha_R$  [20, 21]. The parameter  $\gamma$  is defined by  $\gamma \equiv g\mu_B$  with electron  $g$ -factor  $g$  and Bohr magneton  $\mu_B$ . The electron creation (annihilation) operators around  $+k_F$  and  $-k_F$  are denoted by  $a_{k\sigma}^\dagger$  and  $b_{k\sigma}^\dagger$  ( $a_{k\sigma}$  and  $b_{k\sigma}$ ), respectively. A spin configuration on each Fermi point  $\pm k_F$  depends on a momentum due to the spin-orbit interaction as shown

in Fig. 2, in which the solid lines shows the dispersion relation on the right and left going electrons  $E_R$  and  $E_L$  given by,

$$E_R = v_F (k - k_F) \pm |\alpha_R k_F - \gamma h_y|, \quad (8)$$

$$E_L = -v_F (k + k_F) \pm |\alpha_R k_F + \gamma h_y|. \quad (9)$$

The circles with blue dot and red cross indicate spin direction parallel and anti-parallel to the  $y$ -direction on

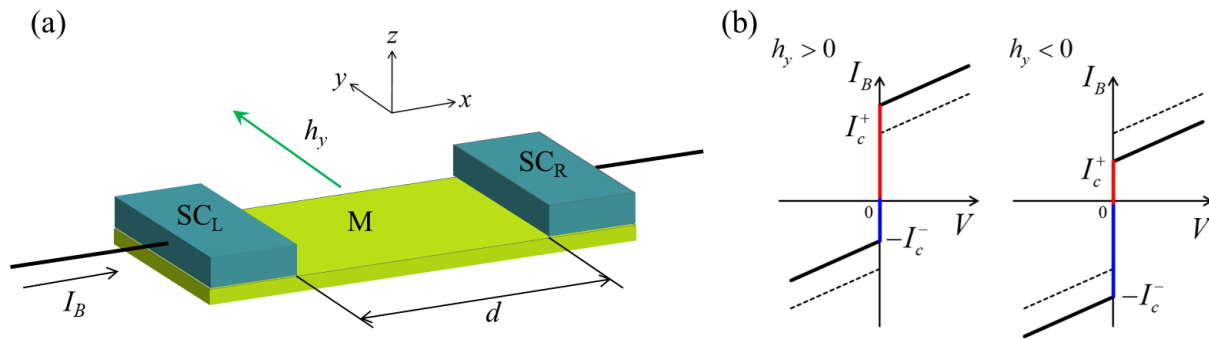


FIG. 1. (a) The device geometry of the Josephson junction through the Rashba system (M). The two SCs ( $SC_R$  and  $SC_L$ ) are separated by the Rashba system with distance  $d$ . An external magnetic field  $h_y$  is applied in the direction perpendicular to the applied current  $I_B$ . The signs of  $I_B$  and  $h_y$  are defined by the Cartesian coordinate shown in this panel. (b) The schematics of the current-voltage curve of the Josephson junction. Due to the Josephson diode effect,  $I_c$  in the positive branch ( $I_c^+$ ) colored by red is different from that in the negative one ( $I_c^-$ ) colored by blue. The broken line is the curve without magnetic field, i.e.,  $h_y = 0$ . For  $h_y > 0$  ( $h_y < 0$ ), the curve is shifted (down) from that with  $h_y = 0$ . The amount of the shift is reversed by reversing  $h_y$ . The Josephson diode effect is characterized by  $I_c^+ - I_c^- \propto I_B \cdot h_y$

each Fermi point, respectively. In the right branch, the blue (red) lines corresponds to the positive (negative) sign of Eq. (8), and in the left branch vice versa with Eq. (9). The dotted broken line shows the dispersion relations without  $\alpha_R$  nor  $h_y$ . The dotted line is split into a couple of blue and red solid lines by  $\alpha_R$ . The splitting of two bands is given by  $2\alpha_R k_F$  for  $h_y = 0$  (upper panel of Fig. 2). Increasing  $h_y$ , the splittings of the left and right

$$E_L = -v_F(k + k_F) \pm |\alpha_R k_F + \gamma h_y| \quad E_R = v_F(k - k_F) \pm |\alpha_R k_F - \gamma h_y|$$

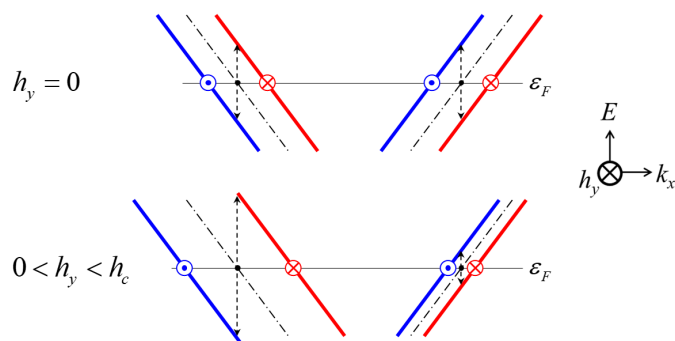


FIG. 2. The magnetic field dependence of the Fermi points in one-dimension. The circles with blue dot and red cross indicate spin direction parallel and anti-parallel to the  $y$ -direction on each Fermi point, respectively. The horizontal thin line denotes the Fermi energy  $\varepsilon_F = v_F k_F$ . The upper panel shows the dispersion relation without an in-plane magnetic field  $h_y$ , which is perpendicular to a  $x$ -direction, and the lower one is for the case of  $0 < h_y < h_c$ , where  $h_c \equiv \alpha_R k_F / \gamma$ .

branches become no longer the same as,  $2|\alpha_R k_F + \gamma h_y|$

for the left, and  $2|\alpha_R k_F - \gamma h_y|$  for the right. In the right branch, the two bands with red and blue merge into one at  $h_y = \alpha_R k_F / \gamma \equiv h_c$  and split again swapping the spin orientation. It should be noted that physical property will not have singularity around  $h_c$ .

The tunneling Hamiltonian  $H_{TL}$  ( $H_{TR}$ ) between  $SC_L$  ( $SC_R$ ) and M is given by,

$$H_{TL} = \sum_{k,q,\sigma=\pm} t \left[ (a_{L,k\sigma}^\dagger + b_{L,k\sigma}^\dagger)(a_{q\sigma} + b_{q\sigma}) + H.c. \right] - \sum_{k,q,\sigma=\pm} t \left[ (a_{L,-k\sigma} + b_{L,-k\sigma})(a_{-q\sigma}^\dagger + b_{-q\sigma}^\dagger) + H.c. \right], \quad (10)$$

$$H_{TR} = \sum_{k,q,\sigma=\pm} t e^{i(k-q)d} \left[ (a_{R,k\sigma}^\dagger + b_{R,k\sigma}^\dagger)(a_{q\sigma} + b_{q\sigma}) + H.c. \right] - \sum_{k,q,\sigma=\pm} t e^{i(k-q)d} \left[ (a_{R,-k\sigma} + b_{R,-k\sigma})(a_{-q\sigma}^\dagger + b_{-q\sigma}^\dagger) + H.c. \right], \quad (11)$$

where the electrode distance between  $SC_L$  and  $SC_R$  is denoted by  $d$ . The tunneling matrix element  $t$  is assumed to be constant.

### III. JOSEPHSON COUPLING ENERGY BETWEEN TWO SUPERCONDUCTORS

The Josephson coupling energy  $F$  is proportional to  $\cos(\phi + \phi_0)$  with a phase difference of SCs  $\phi$  and a constant  $\phi_0$ .  $I_c$  is estimated by the amplitude of the  $\cos \phi$  term. In the fourth order of  $t$  (See Fig. 3),  $F$  is given by,

$$F = \frac{t^4}{4} (\pi \rho_F)^2 \sum_n \frac{|\Delta|^2}{\omega_n^2 + |\Delta|^2} \left[ e^{+i\phi} \sum_{k,k'} \mathcal{A}(k, k') e^{+i(k-k')d} + e^{-i\phi} \sum_{k,k'} \mathcal{A}(k, k') e^{-i(k-k')d} \right], \quad (12)$$

$$\mathcal{A}(k, k') \equiv \sum_{\substack{m=1,2 \\ m'=3,4}} \left\{ g_{m++}(\mathbf{k}') g_{m'--}(-\mathbf{k}) + g_{m--}(\mathbf{k}') g_{m'+++}(-\mathbf{k}) - [g_{m-+}(\mathbf{k}') g_{m'-+}(-\mathbf{k}) + g_{m+-}(\mathbf{k}') g_{m'+-}(-\mathbf{k})] \right\}. \quad (13)$$

with  $\mathbf{k} \equiv (k, i\omega_n)$  and Matsubara frequency of fermion  $\omega_n$ . The prime indicates a different momentum and a different frequency. The Greens functions  $g_{n\alpha\beta}$  ( $n = 1-4$

and  $\alpha, \beta = +, -$ ) is given by,

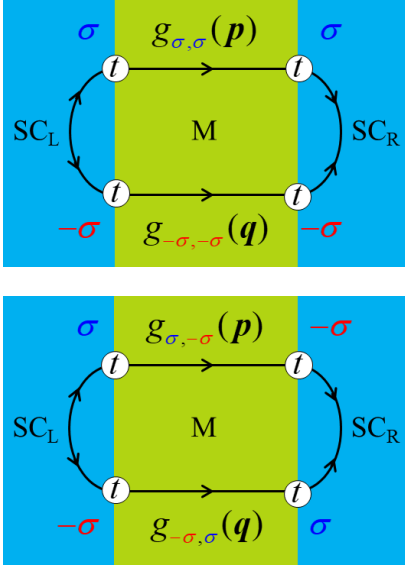


FIG. 3. Diagrams contributing to the Josephson coupling. The Josephson diode effect comes from the process of the lower panel

$$\begin{pmatrix} g_{1++}(\mathbf{k}) & g_{1+-}(\mathbf{k}) \\ g_{1-+}(\mathbf{k}) & g_{1--}(\mathbf{k}) \end{pmatrix} = \frac{1}{(vp + \Lambda_- - i\omega_n)(vp - \Lambda_- - i\omega_n)} \begin{pmatrix} i\omega_n - vp - \gamma h_z & +i\lambda_- \\ -i\lambda_- & i\omega_n - vp + \gamma h_z \end{pmatrix}, \quad (14)$$

$$\begin{pmatrix} g_{2++}(\mathbf{k}) & g_{2+-}(\mathbf{k}) \\ g_{2-+}(\mathbf{k}) & g_{2--}(\mathbf{k}) \end{pmatrix} = \frac{1}{(vq + \Lambda_+ + i\omega_n)(vq - \Lambda_+ + i\omega_n)} \begin{pmatrix} i\omega_n + vq - \gamma h_z & -i\lambda_+ \\ +i\lambda_+ & i\omega_n + vq + \gamma h_z \end{pmatrix}, \quad (15)$$

$$\begin{pmatrix} g_{3++}^*(-\mathbf{k}) & g_{3+-}^*(-\mathbf{k}) \\ g_{3-+}^*(-\mathbf{k}) & g_{3--}^*(-\mathbf{k}) \end{pmatrix} = \frac{1}{(vq + \Lambda_- - i\omega_n)(vq - \Lambda_- - i\omega_n)} \begin{pmatrix} i\omega_n - vq + \gamma h_z & -i\lambda_- \\ +i\lambda_- & i\omega_n - vq - \gamma h_z \end{pmatrix}, \quad (16)$$

$$\begin{pmatrix} g_{4++}^*(-\mathbf{k}) & g_{4+-}^*(-\mathbf{k}) \\ g_{4-+}^*(-\mathbf{k}) & g_{4--}^*(-\mathbf{k}) \end{pmatrix} = \frac{1}{(vp + \Lambda_+ + i\omega_n)(vp - \Lambda_+ + i\omega_n)} \begin{pmatrix} i\omega_n + vp + \gamma h_z & i\lambda_+ \\ -i\lambda_+ & i\omega_n + vp - \gamma h_z \end{pmatrix}, \quad (17)$$

$$\lambda_- \equiv (\alpha_R k_F - \gamma h_y), \quad (18)$$

$$\lambda_+ \equiv (\alpha_R k_F + \gamma h_y). \quad (19)$$

$$vp \equiv v_F (k - k_F), \quad (20)$$

$$vq \equiv v_F (k + k_F). \quad (21)$$

Summing over  $k$  and  $k'$ , Eq. (12) is reduced to,

$$F = -t^4 \mathcal{U} \mathcal{V} \cos \phi, \quad (22)$$

by which  $I_c$  is estimated as  $t^4 \mathcal{U} \mathcal{V}$ . One of prefactors  $\mathcal{U}$  is given by,

$$\mathcal{U} = \left(\frac{2\pi}{v_F}\right)^2 T \sum_n \frac{(\pi\rho_F)^2 \Delta^2}{\omega_n^2 + \Delta^2} e^{-2|\omega_n|d/v_F} \theta(-\omega_n), \quad (23)$$

$$= \left(\frac{2\pi}{v_F}\right)^2 \frac{(\pi\rho_F)^2}{2\Delta^2} \int_0^\infty dx \sin x \left[ \operatorname{cosech} \left( \frac{\pi T x}{\Delta} + \frac{d}{\xi_T} \right) \right], \quad (24)$$

$$\propto \begin{cases} \exp\left(-\frac{d}{\xi_T}\right) & \text{for } d/\xi_T \gg 1 \\ \frac{\xi_0}{d} & \text{for } T \rightarrow 0 \end{cases}, \quad (25)$$

with  $\xi_T \equiv v_F/2\pi T$  and  $\xi_0 \equiv v_F/2\Delta$ . Details to derive Eqs. (24) and (25) are given in Ref. [55]. The factor  $\mathcal{U}$  exponentially decays with  $d$  for  $d/\xi_T \gg 1$  and becomes a power-low decay at low temperatures. The other factor  $\mathcal{V}$ , on the other hand, includes the spin-orbit interaction and is given by,

$$\mathcal{V} = \left[ \cos\left(\frac{\Lambda-d}{v_F}\right) \cos\left(\frac{\Lambda+d}{v_F}\right) - \frac{(\gamma h_z)^2}{\Lambda-\Lambda_+} \sin\left(\frac{\Lambda-d}{v_F}\right) \sin\left(\frac{\Lambda+d}{v_F}\right) \right] + \frac{\lambda_-\lambda_+}{\Lambda-\Lambda_+} \sin\left(\frac{\Lambda-d}{v_F}\right) \sin\left(\frac{\Lambda+d}{v_F}\right), \quad (26)$$

$$\Lambda_\pm \equiv \sqrt{(\gamma h_z)^2 + (\alpha_R k_F \pm \gamma h_y)^2}. \quad (27)$$

This factor Eq. (26) essentially changes the transport property of the Josephson junction, because  $\mathcal{V}$  can be negative, i.e., the  $\pi$ -junction [23, 24]. In Eq. (26), the first and second terms are the contribution of diagonal part, i.e.,  $g_{n++}g_{m--}^* + g_{n--}g_{m++}^*$ , and the last term is the result of the off-diagonal part, i.e.,  $g_{n+-}g_{m-+}^* + g_{n-+}g_{m+-}^*$ , respectively.

For  $h_z = 0$ ,  $h_y = 0$ , and  $\alpha_R \neq 0$ , Eq. (26) becomes constant as,

$$\mathcal{V} = 1. \quad (28)$$

The spin-orbit interaction does not change the coupling between singlet SCs. For  $h_z \neq 0$ ,  $h_y = 0$ , and  $\alpha_R = 0$ , Eq. (26) leads to,

$$\mathcal{V} = \cos\left(\frac{2\gamma h_z d}{v_F}\right), \quad (29)$$

which reproduces the case of the SC/ferromagnet/SC (SFS) junction [23–34, 55]. This is also the case for  $h_z = 0$ ,  $h_y \neq 0$ , and  $\alpha_R \neq 0$ ,

$$\mathcal{V} = \begin{cases} \cos\left[\frac{(\Lambda_+ - \Lambda_-)d}{v_F}\right] & \text{for } \lambda_- > 0 \\ \cos\left[\frac{(\Lambda_+ + \Lambda_-)d}{v_F}\right] & \text{for } \lambda_- < 0 \end{cases} \quad (30)$$

$$= \cos\left(\frac{2\gamma h_y d}{v_F}\right), \quad (31)$$

which is equivalent to Eq. (29) except for the direction of external magnetic field. This is consistent with the previous study by Bezuglyi et al. [22]. The spin-orbit interaction does not appear in the coupling energy in both cases of  $h_z$  and  $h_y$ . The coupling between

singlet SCs is not affected by the spin-orbit interaction in a uniform magnetic field, unless spatial magnetic structure is involved [56–59]. Notably, Eq. (30) has two regions resulting from the topological change of the spin configuration at the Fermi energy (Fig. 2). It is that  $\lambda_- = 0$  corresponds to  $h_y = h_c$ . In spite of the topological change of the spin configuration, the results are identical as Eq. (31) without any singularity.

#### IV. JOSEPHSON DIODE EFFECT DEPENDING ON ELECTRODE DISTANCE

The amplitude of current flowing from one SC to the other through the Rashba system must be identical in each region because of the continuity of electronic current. As a result, the electronic state in the Rashba system is changed to a non-equilibrium steady state. Such a state can be described by the Fermi momentum shift  $q_{ex}$  as,  $+k_F \rightarrow +k_F + q_{ex}/2$  and  $-k_F \rightarrow -k_F + q_{ex}/2$  in the one dimensional model [60]. The current  $I_B$  is generally described by  $I_B = |e|v_d n_e S$  with drift velocity  $v_d$ , electron density  $n_e$ , and cross section  $S$ . It should be noted that  $v_d$  is different from  $v_F$ , e.g.,  $v_d \sim 10^{-3}$  m/s [61]. To bring  $I_B$  into the one-dimensional model, we define a current density per channel by  $i_B \equiv I_B/S$  Ampere(A)/channel with  $S$  in a unit of  $\text{\AA}^2$ . Here we discuss the relation between  $q_{ex}$  and  $i_B$  in our one-dimensional model. The electron density contributing to the current is given by  $n_e = |q_{ex}|/(2\pi)$ , which is a difference of Fermi volume with and without  $i_B$ . Therefore,  $I_B$  is related with  $q_{ex}$  by  $i_B = -|e|v_d q_{ex}/(2\pi)$ . In the experiment, e.g., Ref. [15],  $I_B$  is of the order of 0.1 mA and the cross sectional area  $S = 10 \text{ nm} \times 50 \text{ }\mu\text{m} = 0.5 \times 10^8 \text{ \AA}^2$ . Therefore, we can estimate as  $q_{ex} = -2\pi i_B / (|e|v_d) \sim 4 \text{ \AA}^{-1}$ , which

is of the same order of  $k_F$ . In our theory,  $q_{ex}/k_F < 1$  is necessary because of the linearized dispersion relation.

The current-voltage curve of the Josephson junction is obtained by biasing the junction with current and measuring the voltage. Under the current bias,  $\lambda_-$  and  $\lambda_+$

in Eqs.(18) and (19) are substituted by,

$$\lambda'_- = \alpha_R (k_F + q_{ex}/2) - \gamma h_y, \quad (32)$$

$$\lambda'_+ = \alpha_R (k_F - q_{ex}/2) + \gamma h_y. \quad (33)$$

The coupling energy under the current bias  $F_{bias}$  in the fourth order of  $t$  is given by,

$$F_{bias} = -t^4 \mathcal{U} \mathcal{V}_{bias} \cos(\phi + q_{ex}d), \quad (34)$$

$$\begin{aligned} \mathcal{V}_{bias} &= \mathcal{V} + \frac{q_{ex}}{k_F} \frac{\alpha_R k_F}{\Lambda_- \Lambda_+} \frac{\gamma h_y}{\hbar v_F} \sin\left(\frac{\Lambda'_+ d}{\hbar v_F}\right) \sin\left(\frac{\Lambda'_- d}{\hbar v_F}\right) - \frac{\alpha_R^2 q_{ex}^2}{4\Lambda_- \Lambda_+} \sin\left(\frac{\Lambda_- d}{\hbar v_F}\right) \sin\left(\frac{\Lambda_+ d}{\hbar v_F}\right), \\ &\equiv \mathcal{V} + \delta\mathcal{V}_o - \delta\mathcal{V}_e, \end{aligned} \quad (35)$$

where  $\hbar$  is explicitly written to discuss a length scale below. It should be noted that the amplitude of the cosine term in Eq. (34) is modified by the  $q_{ex}$ , i.e.,  $i_B$ . The second term of Eq. (35),  $\delta\mathcal{V}_o$ , represents the Josephson diode effect,

$$I_c^+ - I_c^- = 2t^4 \mathcal{U} \delta\mathcal{V}_o \propto \alpha_R \cdot i_B \cdot h_y, \quad (36)$$

where  $q_{ex} = -2\pi i_B / |e|v_d$  is used [63]. The Josephson diode effect requires three factors, i.e.,  $\alpha_R$ ,  $i_B$ , and  $h_y$ . Since the term is proportional to their product  $\alpha_R \cdot i_B \cdot h_y$ , the change of  $I_c$ , i.e.,  $I_c^+ - I_c^-$ , due to the applied current is odd with respect to a direction of the current or an external magnetic field as is observed in the experiments. More importantly, the Josephson diode effect depends on  $d$  as well as  $i_B$  and  $h_y$  due to the term,  $\sin(\Lambda_- d / \hbar v_F) \sin(\Lambda_+ d / \hbar v_F)$ , in Eq. (35). The  $d$ -dependence of the Josephson diode effect is the important finding of this study and has not been mentioned so far.

The length scale of the Josephson diode effect is determined by  $\Lambda_{\pm}$  composed of  $\alpha_R k_F$ ,  $\gamma h_y$ , and  $\gamma h_z$ . The  $\alpha_R k_F$  corresponds to the band splitting at the Fermi surface and its magnitude ranges from sub meV to several hundreds meV depending on materials and their form, e.g., bulk, film or surface [64–66]. The magnitude of  $\gamma h_z$  and  $\gamma h_y$  is usually up to 10 T that corresponds to about 1 meV. Using a typical value of  $v_F \sim 10^6$  m/s [62] and  $d$  in units of nm, the length scale is determined by  $d / \hbar v_F \sim 1.52d$  eV<sup>-1</sup>. Below, we consider the case of  $h_y = 10$  T and  $h_z = 0$  T.

The efficiency of the Josephson diode effect,  $Q$ , is defined by  $Q \equiv (I_c^+ - I_c^-) / (I_c^+ + I_c^-)$ . In our theory, it gives,

$$Q = \frac{\delta\mathcal{V}_o}{\mathcal{V} + \delta\mathcal{V}_e}, \quad (37)$$

$$\sim \frac{q_{ex}}{k_F} \frac{\gamma h_y}{\alpha_R k_F} \frac{1}{2} \left[ 1 - \frac{\cos(2\gamma h_y d / \hbar v_F)}{\cos(2\alpha_R k_F d / \hbar v_F)} \right], \quad (38)$$

where terms in the order of  $(\gamma h_y / \alpha_R k_F)^2$  are not shown. In Fig. 4,  $Q$  is plotted in units of  $q_{ex}/k_F$  for (a)  $\alpha_R k_F = 5$

meV (green), 10 meV (blue), and 20 meV (red); (b)  $\alpha_R k_F = 20$  meV (red), 50 meV (light green), and 100 meV (black). The rectangular area in (a) denoted by the broken line corresponds to the plot area of (b). The red lines in (a) and (b) are identical except for the plot area. The magnitude of  $Q$  oscillates with  $d$  and changes its sign. It means that the Josephson diode effect can be optimized by tuning of  $d$ . This provides a guiding principle for the Josephson diode device, because  $d$  can be controlled in experiments. It is also important that the Josephson diode effect changes its sign with  $d$ , even when  $\alpha_R$ ,  $q_{ex}$  and  $h_y$  are fixed. To determine not only the magnitude of the Josephson diode effect, but also its sign, we must take care of  $d$  as well.

Increasing  $\alpha_R k_F$ , the period of the oscillation becomes short and the magnitude is suppressed. This can be understood by Eq. (35),

$$\delta\mathcal{V}_o \sim \frac{1}{2} \frac{q_{ex}}{k_F} \frac{\gamma h_y}{\alpha_R k_F} \left[ \cos\left(\frac{2\gamma h_y d}{\hbar v_F}\right) - \cos\left(\frac{2\alpha_R k_F d}{\hbar v_F}\right) \right]. \quad (39)$$

for  $\alpha_R k_F \gg h_y$  and  $h_z = 0$ . In Fig. 4, since  $\gamma h_y = 1$  meV is used, the second term of Eq. (39) dominates the  $d$ -dependence of  $Q$  and the first term is almost 1 in the area of Fig. 4. Equation (39) is a decreasing function with respect to  $\alpha_R k_F$ . Therefore, the Josephson diode effect becomes smaller for larger values of  $\alpha_R k_F$  as shown in Fig. 5. Although the spin-orbit interaction is necessary for the Josephson diode effect, larger  $\alpha_R$  does not always results in a larger effect. Sometimes the effect may accidentally disappear, e.g.,  $\alpha_R k_F \sim 20$  meV in Fig. 5. In general, it is not easy to tune  $\alpha_R k_F$ , whereas  $d$  can be controlled in experiment. Our results suggests that the Josephson diode effect can be optimized by tuning of  $d$ .

## V. SUMMARY

We theoretically studied the Josephson diode effect in the Josephson junction with singlet superconductors sep-

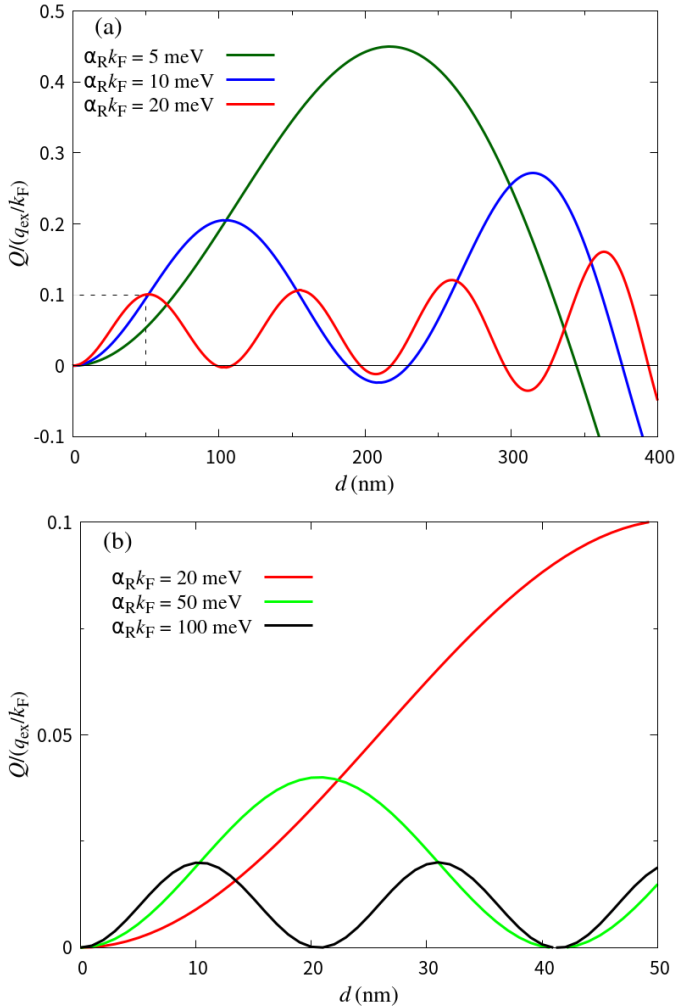


FIG. 4. The  $d$ -dependence of  $Q$  in units of  $q_{ex}/k_F$  with  $h_y = 10$  T and  $h_z = 0$  T is plotted for (a)  $\alpha_R k_F = 5$  meV (green), 10 meV (blue), and 20 meV (red); (b)  $\alpha_R k_F = 20$  meV (red), 50 meV (light green), and 100 meV (black). The rectangular area in (a) denoted by the broken line corresponds to the plot area of (b). The red lines in (a) and (b) are the same line except for the plot area.

arated by the Rashba system. The coupling energy of two superconductors was formulated under the bias current using a tunneling Hamiltonian with a one-dimensional model. The Josephson diode effect occurs as the response to the bias current. Therefore, including the bias current into the formulation is important to study the Josephson diode effect. The bias current is included in our formulation as the shifts of the Fermi momentum in the Rashba system. Due to the shift of Fermi momentum, the critical current is asymmetrically changed with respect to the current and the magnetic field. By including the bias current in the formulation, the first harmonic of the Josephson coupling can reproduce the Josephson diode effect. More importantly, the Josephson diode effect depends on the distance between superconducting electrodes  $d$ .

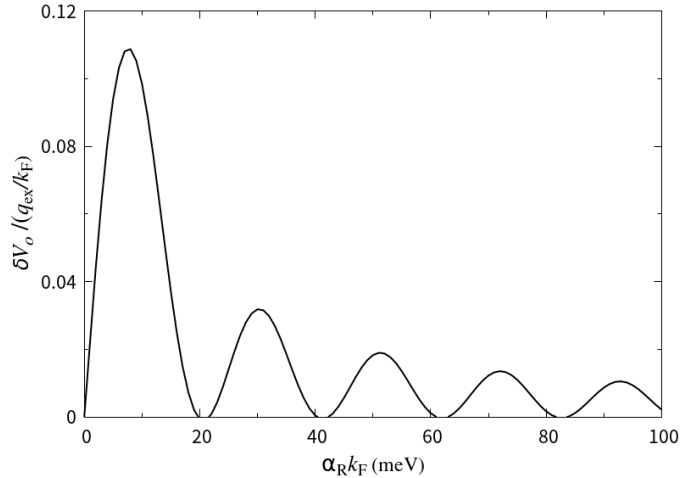


FIG. 5. The  $\alpha_R k_F$ -dependence of  $\delta V_o$  with  $d = 100$  nm, and  $h_y = 10$  T,  $h_z = 0$  T.

In general, it is difficult to tune the band splitting by the spin-orbit interaction, whereas  $d$  is experimentally controllable. Our findings suggest that the Josephson diode effect can be optimized by tuning of  $d$ . It will help to observe the Josephson diode effect experimentally. The magnitude of the Josephson diode effect is inversely proportional to the band split at the Fermi surface caused by the spin-orbit interaction. Although the spin-orbit interaction is necessary, larger  $\alpha_R$  does not always result in a larger effect. Our theory develops a new guiding principle to design the Josephson diode device.

## ACKNOWLEDGMENTS

This work was supported by JSPS Grant Nos. JP20K03810, JP21H04987, JP23K03291 and the inter-university cooperative research program (No. 202312-CNKXX-0016) of the Center of Neutron Science for Advanced Materials, Institute for Materials Research, Tohoku University. WK was supported by CREST Grant No. JPMJCR20T1 from JST. SM was supported by JSPS Grant No. JP24K00576. A part of the computations were performed on supercomputers at the Japan Atomic Energy Agency.

## Appendix A: Current-phase relation

The Josephson coupling energy under a current bias has not been formulated by the tunneling Hamiltonian. It is noted that  $q_{ex}$  in Eq. (34) is a function of  $i_B$  as discussed in Sec. IV, i.e.,  $q_{ex} = -2\pi i_B / |e|v_d$ . Taking the derivative with respect to  $\phi$  over the sum of Eq. (34) and

the external force  $i_B \cdot \phi$ , we obtain the equation,

$$i_B = t^4 \mathcal{U} \mathcal{V}_{bias} \sin \left( \phi - \frac{2\pi d}{|e|v_d} i_B \right). \quad (\text{A1})$$

Solving Eq. (A1) with respect to  $i_B$ , the current-phase relation under the current bias is obtained as shown in Fig. 6, in which Eq. (A1) is parameterized by  $x \equiv \phi$ ,

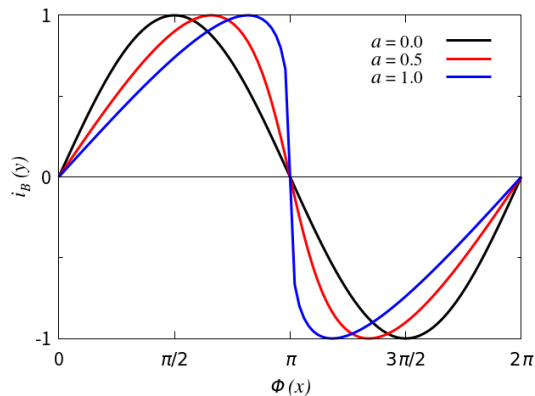


FIG. 6. The current-phase relation obtained by solving  $y = \sin(x - a \cdot y)$  which is reduced from Eq. (A1) with  $y \equiv i_B$ ,  $x \equiv \phi$ ,  $a \equiv 2\pi d/|e|v_d$ , and  $t^4 \mathcal{U} \mathcal{V}_{bias} = 1$ .

$y \equiv i_B$ , and  $a \equiv 2\pi d/|e|v_d$  and is reduced to  $y = \sin(x - a \cdot y)$  with  $t^4 \mathcal{U} \mathcal{V}_{bias} = 1$ . The current-phase relation is modified as that of metallic interface by increasing  $a$ . When the parameter  $a$  is much larger than 1, the current-phase relation deviates from the sinusoidal behavior. Since we adopted the one-dimensional model for the two-dimensional system, we cannot exactly assign the value of  $a$ . For studying the Josephson diode effect, we assumed that the current phase relation is a periodic function like that in Fig. 6. Although the exact formulation of the current-phase relation under the current bias is not the main purpose of this study, it is also interesting and will be numerically studied using the two-dimensional system elsewhere in future.

- 
- [1] A. M. Kadin, R. Burkhardt, J. D. Chen, J. E. Keem, and S. R. Ovshinsky, *Proceedings of the 17th International Conference on Low Temperature Physics, LT 17, Karlsruhe* (North-Holland, Amsterdam, 1984), p. 579.
- [2] P. R. Broussard and T. H. Geballe, *Phys. Rev. B* **37**, 68 (1988).
- [3] N. Touthou, P. Bernstein, J.F. Hamet, Ch. Simon, L. Méchin, J.P. Contour, and E. Jacquet, *Appl. Phys. Lett.* **85**, 1742 (2004).
- [4] F. Ando, Y. Miyasaka, T. Li, J. Ishizuka, T. Arakawa, Y. Shiota, T. Moriyama, Y. Yanase, and T. Ono, *Nature* **584**, 7821 (2020).
- [5] Y. Miyasaka, R. Kawarazaki, H. Narita, F. Ando, Y. Ikeda, R. Hisatomi, A. Daido, Y. Shiota, T. Moriyama, Y. Yanase, and T. Ono *Appl. Phys. Express* **14**, 073003 (2021).
- [6] R. Kawarazaki, H. Narita, Y. Miyasaka, Y. Ikeda, R. Hisatomi, A. Daido, Y. Shiota, T. Moriyama, Y. Yanase, A.V. Ognev, A.S. Samardak, and T. Ono, *Appl. Phys. Express* **15**, 113001 (2022).
- [7] H. Narita, J. Ishizuka, R. Kawarazaki, D. Kan, Y. Shiota, T. Moriyama, Y. Shimakawa, A.V. Ognev, A.S. Samardak, Y. Yanase, and T. Ono, *Nature Nanotech.* **17**, 823–828 (2022).
- [8] Y. Hou, F. Nichele, H. Chi, A. Lodesani, Y. Wu, M.F. Ritter, D.Z. Haxell, M. Davydova, S. Ilić, O. Glezakou-Elbert, A. Varambally, F.S. Bergeret, A. Kamra, L. Fu, P.A. Lee, and J.S. Moodera, *Phys. Rev. Lett.* **131**, 027001 (2023).
- [9] V. M. Edelstein, *J. Phys. Cond. Matt.* **8**, 339 (1996).
- [10] A. Daido, Y. Ikeda, and Y. Yanase, *Phys. Rev. Lett.* **128**, 037001 (2022).
- [11] J. J. He, Y. Tanaka, and N. Nagaosa, *New J. Phys.* **24**, 053014 (2022).
- [12] N. F. Q. Yuan and L. Fu, *PNAS* **119**, e2119548119 (2022).
- [13] K. Aoyama, *Phys. Rev. B* **109**, 024516 (2024).
- [14] C. Baumgartner, L. Fuchs, A. Costa, S. Reinhardt, S. Gronin, G. C. Gardner, T. Lindemann, M. J. Manfra, P. E. F. Junior, D. Kochan, J. Fabian, N. Paradiso, and C. Strunk, *Nat. Nanotech.* **17**, 1 (2022).
- [15] K.-R. Jeon, J.-K. Kim, J. Yoon, J.-C. Jeon, H. Han, A. Cottet, T. Kontos, and S. S. P. Parkin, *Nature Mater.* **21**, 1008 (2022).
- [16] B. Pal, A. Chakraborty, P.K. Sivakumar, M. Davydova, A.K. Gopi, A. K. Pandeya, J.A. Krieger, Y. Zhang, M. Date, S. Ju, N. Yuan, N. B. M. Schröter, L. Fu, and S. S. P. Parkin, *Nat. Phys.* **18**, 1228 (2022).
- [17] H. Wu, Y. Wang, Y. Xu, P.K. Sivakumar, C. Pasco, U. Filippozzi, S. S. P. Parkin, Y.-J. Zeng, T. McQueen, and M. N. Ali, *Nature* **604**, 653 (2022).
- [18] J.-K. Kim, K.-R. Jeon, P. K. Sivakumar, J. Jeon, C. Koerner, G. Woltersdorf, and S. S. P. Parkin, *Nature Commun.* **15**, 1120 (2024).
- [19] E. Nikodem, J. Schluck, M. Geier, M. Papaj, H. F. Legg, J. Feng, M. Bagchi, L. Fu, and Y. Ando, *arXiv:2412.16569*.
- [20] E. I. Rashba, *Sov. Phys. Solid State* **2** 1109 (1960).
- [21] Yu. A. Bychkov and E. I. Rashba, *JETP Lett.* **39**, 78 (1984).



- [22] E. V. Bezuglyi, A. S. Rozhavsky, I. D. Vagner, and P. Wyder, Phys. Rev. B **66**, 052508 (2002).
- [23] L. N. Bulaevskii, V. V. Kuzii, and A. A. Sobyenin, JETP Lett. **25**, 290 (1977).
- [24] A. I. Buzdin, L. N. Bulaevskii, and S. V. Panyukov, JETP Lett. **35**, 178 (1982).
- [25] V. V. Ryazanov, V. A. Oboznov, A. Yu. Rusanov, A. V. Veretennikov, A. A. Golubov, and J. Aarts, Phys. Rev. Lett. **86**, 2427 (2001).
- [26] T. Kontos, M. Aprili, J. Lesueur, F. Genêt, B. Stephanidis, and R. Boursier, Phys. Rev. Lett. **89**, 137007 (2002).
- [27] H. Sellier, C. Baraduc, F. Lefloch, and R. Calemczuk, Phys. Rev. B **68**, 054531 (2003).
- [28] S. M. Frolov, D. J. Van Harlingen, V. A. Oboznov, V. V. Bolginov, and V. V. Ryazanov, Phys. Rev. B **70**, 144505 (2004).
- [29] C. Bell, R. Loloee, G. Burnell, and M. G. Blamire, Phys. Rev. B **71**, 180501R (2005).
- [30] V. A. Oboznov, V. V. Bolginov, A. K. Feofanov, V. V. Ryazanov, and A. I. Buzdin, Phys. Rev. Lett. **96**, 197003 (2006).
- [31] V. Shelukhin, A. Tsukernik, M. Karpovskii, Y. Blum, K. B. Efetov, A. F. Volkov, T. Champel, M. Eschrig, T. Loefwander, G. Schoen, and A. Palevski, Phys. Rev. B **71**, 174506 (2006).
- [32] J. W. A. Robinson, S. Piano, G. Burnell, C. Bell, and M. G. Blamire, Phys. Rev. Lett. **97**, 177003 (2006).
- [33] F. Born, M. Siegel, E. K. Hollmann, H. Braak, A. A. Golubov, D. Yu. Gusakova and M. Yu. Kupriyanov: Phys. Rev. B **74**, 140501 (2006).
- [34] M. Weides, M. Kemmler, H. Kohlstedt, R. Waser, D. Koele, R. Kleiner, and E. Goldobin: Phys. Rev. Lett. **97**, 247001 (2006).
- [35] T. Yamashita, K. Tanikawa, S. Takahashi, and S. Maekawa, Phys. Rev. Lett. **95** (2005) 097001
- [36] T. Yamashita, S. Kim, H. Kato, W. Qiu, K. Semba, A. Fujimaki, and H. Terai, Sci. Rep. **10**, 13687 (2020).
- [37] A. Buzdin, Phys. Rev. Lett. **101**, 107005 (2008).
- [38] T. Yokoyama, M. Eto, and Y. V. Nazarov, Phys. Rev. B **89**, 195407 (2014).
- [39] Y. Zhang, Y. Gu, P. Li, J. Hu, and K. Jiang, Phys. Rev. X **12**, 041013 (2022).
- [40] M. Davydova, S. Prembabu, and L. Fu, Science Adv. **8**, eabo0309 (2022).
- [41] R. S. Souto, M. Leijnse, and C. Schrade, Phys. Rev. Lett. **129**, 267702 (2022).
- [42] Y. Tanaka, B. Lu, and N. Nagaosa, Phys. Rev. B **106**, 214524 (2022).
- [43] B. Lu, S. Ikegaya, P. Buset, Y. Tanaka, and N. Nagaosa, Phys. Rev. Lett. **131**, 096001 (2023).
- [44] J.-X. Hu, Z.-T. Sun, Y.-M. Xie, and K. T. Law, Phys. Rev. Lett. **130**, 266003 (2023).
- [45] P.-H. Fu, Y. Xu, S. A. Yang, C. H. Lee, Y. S. Ang, and J.-F. Liu, Phys. Rev. Appl. **21**, 054057 (2024).
- [46] J. Cayao, N. Nagaosa, and Y. Tanaka, Phys. Rev. B **109**, L081405 (2024).
- [47] D. Debnath and P. Dutta, Phys. Rev. B **109**, 174511 (2024).
- [48] A. Soori, J. Phys. Cond. Mat. **36**, 335303 (2024).
- [49] S. Fracassi, S. Traverso, N. Traverso Ziani, M. Carrega, S. Heun, and M. Sassetti, Appl. Phys. Lett. **124**, 242601 (2024).
- [50] Y. Yerin, S.-L. Drechsler, A. A. Varlamov, M. Cuoco, and F. Giazotto, Phys. Rev. B **110**, (2024).
- [51] S. Ilić, P. Virtanen, D. Crawford, T. T. Heikkilä, and F. S. Bergeret, Phys. Rev. B **110**, L140501 (2024).
- [52] A. Soori, J. Phys. Cond. Mat. **37**, 10LT02 (2025).
- [53] D. Debnath and P. Dutta, arXiv:2411.18325.
- [54] In the vector representation, it should be  $\vec{I}_B \times \vec{h}$ . In this paper,  $I_B \parallel x$  and  $h_y \parallel y$  are scalar.
- [55] M. Mori, S. Hikino, S. Takahashi, and S. Maekawa, J. Phys. Soc. Jpn. **76**, 054705 (2007).
- [56] F. S. Bergeret, A. F. Volkov, and K. B. Efetov, Phys. Rev. B **64**, 134506 (2001).
- [57] V. N. Krivoruchko and R. V. Petryuk, Phys. Rev. B **66**, 134520 (2002).
- [58] S. Mironov, A. Mel'nikov, and A. Buzdin, Phys. Rev. Lett. **109**, 237002 (2012).
- [59] A. S. Mel'nikov, S. V. Mironov, A. V. Samokhvalov, and A. I. Buzdin, Phys. Uspekhi **65**, 1248 (2022).
- [60] The electronic current must be continuous through the junction. The total amount of current flowing in the superconductor has to be equal to that in the Rashba system. In order to understand the relation between  $q_{ex}$  and the supercurrent, it is useful to consider the conventional Josephson junction, i.e., the superconductor/insulator/superconductor (SIS) junction. The supercurrent in the SIS junction is related to the phase difference, which is equivalent to the magnetic flux, since the supercurrent is the diamagnetic current. This can be interpreted as: There is a vector potential between the left and right superconductors. In the junction via the Rashba system, on the other hand, the current flows in the Rashba system under the same condition as the SIS junction. It means that the vector potential is added to the Rashba system due to the phase difference between two superconductors. If a supercurrent flows in a junction with a phase difference, the same amount of current flows in the Rashba system due to the continuity of the current. Since the current is related to the vector potential, the momentum of electrons is shifted by the vector potential. Therefore, the shift of the Fermi momentum  $q_{ex}$  is necessary to satisfy the continuity of the electronic current through the junction.
- [61] We consider a current  $I$  with 1 [A] flowing in a wire with 1 [mm] radius. For copper, using  $n_e \sim k_F^3/3\pi^2 \sim 10^{22}$  [cm<sup>-3</sup>] [62], it is estimated that  $v_d = I/(|e|n_e S) \sim 10^{-3}$  [m/s]. For another case with small electron density such as GaAs with  $n_e \sim 10^{17}$  [cm<sup>-3</sup>],  $v_d = I/(|e|n_e S) \sim 10^2$  [m/s]. In fact,  $v_d$  is much smaller than  $v_F$ . On the other hand,  $v_d$  will depend on materials and geometry, e.g., interface and surface.
- [62] N. W. Ashcroft and N. D. Mermin, *Solid State Physics* (Thomson Learning, USA, 1976) Chap. 2, p. 38.
- [63] The phase factor as a function of  $k - k'$  in Eq. (12) leads to  $\cos(\phi + q_{ex}d)$  and  $\mathcal{V}_{bias}$ . To summarize the long calculation briefly, it is found that the center of mass momentum of Cooperon in the Rashba system is given by,  $k_\uparrow - k'_\downarrow \sim q_{ex} + 2\gamma h_z/v_F$  and  $k_\downarrow - k'_\uparrow \sim q_{ex} - 2\gamma h_z/v_F$ , where  $k_\uparrow$  and  $k_\downarrow$  corresponds to the momentum in  $g_{m++}(k)$  and  $g_{m--}(k)$ , respectively. Both of  $h_y$  and  $q_{ex}$  shift the center of mass momentum of Cooperon. However,  $h_y$  shifts the momentum out-of-phase, while  $q_{ex}$  does it in-phase. Due to this difference,  $h_y$  leads to  $\cos(2\gamma h_z d/v_F)$  explaining the  $\pi$ -junction, while  $q_{ex}$  shifts the phase difference as  $\cos(\phi + q_{ex}d)$ .

- [64] S. LaShell, B. A. McDougall, and E. Jensen, *Phys. Rev. Lett.* **77**, 3419 (1996).
- [65] C. R. Ast, J. Henk, A. Ernst, L. Moreschini, M. C. Falub, D. Pacilé, P. Bruno, K. Kern, and M. Grioni, *Phys. Rev. Lett.* **98**, 186807 (2007).
- [66] K. Ishizaka, M.S. Bahrany, H. Murakawa, M. Sakano, T. Shimojima, T. Sonobe, K. Koizumi, S. Shin, H. Miyahara, A. Kimura, K. Miyamoto, T. Okuda, H. Namatame, M. Taniguchi, R. Arita, N. Nagaosa, K. Kobayashi, Y. Murakami, R. Kumai, Y. Kaneko, Y. Onose, and Y. Tokura, *Nature Mater.* **10**, 521 (2011).